Potent Angiogenesis Inhibition by the Particulate Form of Fullerene Derivatives

Huan Meng,[†,⊥] Gengmei Xing,[†,⊥] Baoyun Sun,[†] Feng Zhao,[†] Hao Lei,[‡] Wei Li,[†] Yan Song,[†] Zhen Chen,[†] Hui Yuan,[†] Xuxia Wang,[‡] Jing Long,[†] Chunying Chen,[†] Xingjie Liang,[†] Ning Zhang,[§] Zhifang Chai,[†] and Yuliang Zhao[†,§,*]

[†]CAS Key Laboratory for Biomedical Effects of Nanomaterials & Nanosafety, Institute of High Energy Physics, Chinese Academy of Sciences, Beijing 100049, and National Center for Nanosciences and Technology of China, Beijing 100190, China, [‡]State Key Laboratory of Magnetice Resonance and Atomic and Molecular Physics, Wuhan Institute of Physics and Mathematics, Chinese Academy of Sciences, Wuhan 430071, China, and [§]Research Center for Cancer Nanotechnology, Tianjin Cancer Hospital and Chinese Academy of Sciences, Tianjin 300060, China. [⊥]These authors contributed equally to this work.

ABSTRACT Antiangiogenesis is an effective strategy for cancer treatment because uncontrolled tumor growth depends on tumor angiogenesis and sufficient blood supply. Great progress has been made in developing a "molecular" form of angiogenesis inhibitors; however, the narrow inhibition spectrum limits anticancer efficacy as those inhibitors that usually target a few or even a single angiogenic factor among many angiogenic factors might initially be effective but ultimately lead to the failure of the treatment due to the induction of expression of other angiogenic factors. In this work, we report that with a multiple hydroxyl groups functionalized surface, the $Gd@C_{82}(OH)_{22}$ fullerenic nanoparticles (f-NPs) are capable of simultaneously downregulating more than 10 angiogenic factors in the mRNA level that is further confirmed at the protein level. After studying this antiangiogenesis activity of the f-NPs by cellular experiment, we further investigated its anticancer efficacy *in vivo*. A two-week treatment with the f-NPs decreased >40% tumor microvessels density and efficiently lowered the speed of blood supply to tumor tissues by ~40%. Efficacy of the treatment using f-NPs in nude mice was comparable to the clinic anticancer drug paclitaxel, while no pronounced side effects were found. These findings indicate that the f-NPs with multiple hydroxyl groups serve as a potent antiangiogenesis inhibitor that can simultaneously target multiple angiogenic factors. We propose that using nanoscale "particulate" itself as a new form of medicine (particulate medicine) may be superior to the traditional "molecular" form of medicine (molecular medicine) in cancer treatment.

KEYWORDS: $Gd@C_{82}(OH)_{22}$ fullerene nanoparticle · particulate form of medicine · tumor angiogenesis

Tumor-associated angiogenesis refers to the growth of new vessels toward and within the tumor.[1] This is essential for the growth and persistence of solid tumors and their metastases because malignant carcinoma diseases need sufficient blood supply to maintain the rapid growth that eventually becomes incontrollable.[1] As the tumor angiogenesis is regulated by a variety of angiogenic factors, rather than direct cancer cell killing, one important strategy in achieving efficient cancer growth inhibition is to suppress these angiogenic factors.[2,3] Great progress has been made in discovery of angiogenesis inhibitors including small molecules inhibitor,[4] peptide inhibitor,[5] and antibody-based inhibitor.[6] However, the applications of these angiogenesis inhibitors in "molecular" form are accompanied by several issues of limiting anticancer efficacy. They usually target a few or even a single angiogenic factor, might initially be effective, but ultimately lead to the failure of treatment because the narrow inhibition spectrum usually selects for tumor cells that overexpress other angiogenic factors as an alternative.[7] This may raise the possibility of drug resistance in cancer treatment that uses an angiogenesis inhibitor for a long time period. Other problems, such as a poor pharmacokinetics profile, unsatisfied stability, and side-effects, *etc.*, may also limit the clinical application.[7,8] For example, the treatment using angiogenesis inhibitor likely lasts for a relatively long time because the angiogenesis inhibitor may not necessarily directly kill cancer *via* cytotoxicity, and is therefore accompanied by a series of problems with bleeding, blood clotting, and the reproductive system.[7] These pitfalls highlight the need for discovering a new generation of angiogenesis inhibitor capable of simultaneously inhibiting multiple angiogenic factors or development of new drug delivery system for those existing inhibitors.

To explore the solution for this important need, we considered an anticancer drug in "particulate" form. Compared with conventional medicine of "molecular" form, "particulate" form, like a nanoparticle that has versatile surface and controllable size distribution, is easily functionalized and may interact with biosystems in a more effective fashion to regulate biological processes in disease development.[9−12] The forces controlling physicochemical activities of a nanoparticle are similar to those directing biological activities of a molecule or

*Address correspondence to zhaoyuliang@ihep.ac.cn.

Received for review March 4, 2010 and accepted April 21, 2010.

Published online April 29, 2010.
10.1021/nn100448z

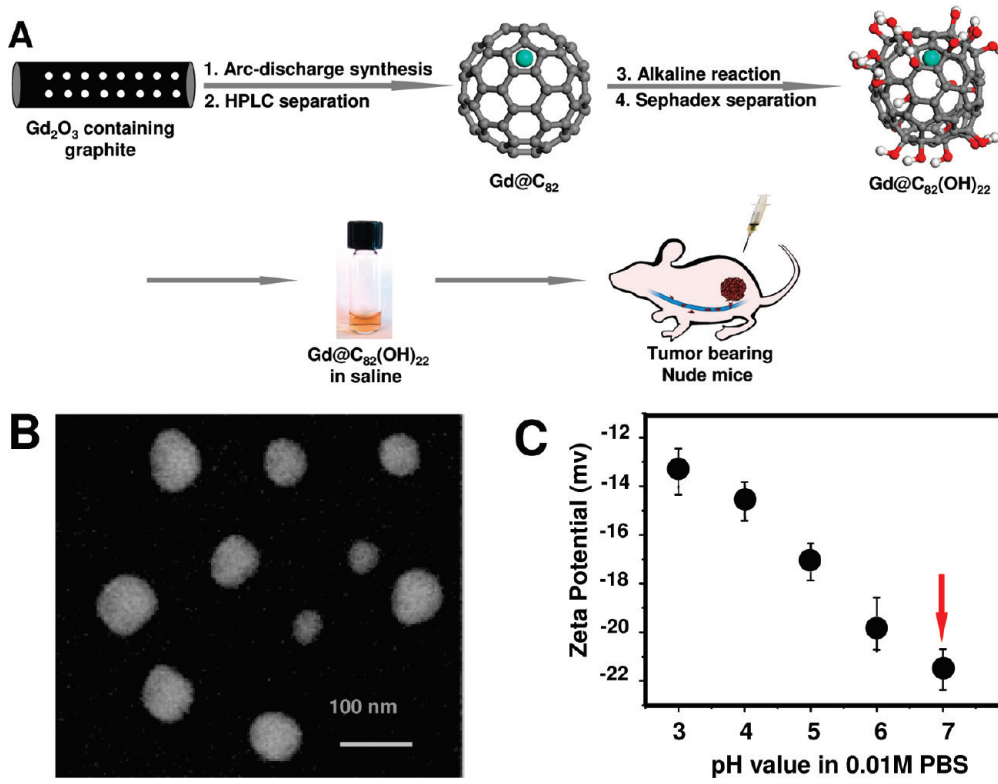

Figure 1. Synthesis and characterization of the f-NPs. (A) The synthesis processes and structure of $Gd@C_{82}(OH)_x$ ($x = 20-24$), and its saline solution. $Gd@C_{82}(OH)_{22}$ saline solution was used in following biological experiment. (B) SEM image for the f-NPs. (C) Zeta potential of the f-NPs in PBS with various pH values ranging from 3 to 8.

complex in biosystems, such as hydrogen bonds, van der Waals forces, hydrophobic−hydrophilic interactions, or static interactions.[9] People therefore envisage a major breakthrough in disease treatment *via* utilizing the interactions between nanosystems and biosystems that occur at spatial dimension of a nanoscale.[9,13] Recently, hydroxylated metallofullerenes (metallofullerenols) have shown attractive applications in biomedicines, including radiotracers,[14] magnetic resonance imaging (MRI) contrast agents,[15] and in particular as a pharmaceutically active nanomaterial in anticancer treatment.[16] In 2005, we first reported that the $Gd@C_{82}(OH)_{22}$ nanopaticles (f-NPs) potently prevented tumor proliferation in a rodent carcinoma model (H22 hepatocellular carcinoma) while the mechanisms behind it still remained unclear.[16] High-content or high-rapid screening technologies (*e.g.*, gene-array, molecular simulation) were subsequently used to provide us "clues" in revealing the mechanisms hidden behind the exciting findings. In this follow-up study, we established the link between the potent anticancer activity to the poor tumor angiogenesis along with the f-NPs treatment, suggesting this particle served as an effective antiangiogenesis inhibitor in "particulate" form. The f-NPs potently inhibit tumor angiogenesis by the simultaneous downregulation of more than 10 angiogenic factors, resulting in insufficient tumor blood perfusion, and yielding a high-efficient cancer inhibition rate without detectable side-effects in tumor bearing nude mice.

RESULTS

Characterization of the f-NPs. Synthesis procedures together with the unique structural and surface features of the f-NPs are schemed in Figure 1A. The f-NPs consist of an innermost core of gadolinium (Gd) atom and

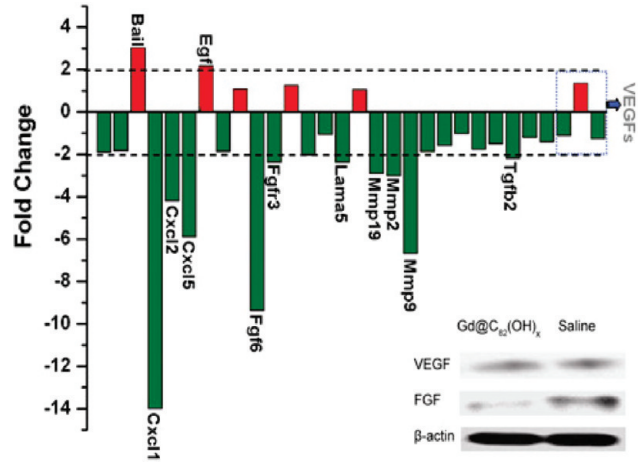

Figure 2. The f-NPs simultaneously downregulated multiple angiogenic factors on the mRNA level: analysis of expression of angiogenic factors in tumors with the f-NP treatment by quantitative PCR-array. The *Y*-axis indicates the fold changes when compared to saline control. Some of the factors, including FGF and VEGF, were confirmed on the protein level by Western blotting assay.

an outer sheath of carbon atoms which are further modified by 22 outermost hydroxyl groups. They were then characterized for morphology and size by scanning electron microscope (SEM) (Figure 1B), showing an average diameter of 72 ± 18 nm. To conduct biological experimentation, zeta potential was measured in saline with a series of pH values that ranged from 3 to 8. The f-NPs exhibited a negative zeta potential at all the pH conditions, the lowest zeta value (−22 mV) was observed in a neutral pH environment, suggesting a high stability and good dispersion in biological system (Figure 1C). Further characterization data, including time-of-flight mass spectrometry (MALDI-TOF-MS) and determination of −OH number were summarized in the Supporting Information section S1.

The f-NPs Simultaneously Downregulated Multiple Angiogenic Factors. Our preliminary data have shown a strong capacity on tumor growth inhibition in a murine cancer model after f-NP treatment; however, little is known on the anticancer mechanism of this pharmaceutically active nanomaterial.[16] Unlike cytotoxic chemotherapeutic agents, the f-NPs do not directly kill cancer cells. We therefore propose that an "indirect" tumor inhibition mechanism may get involved along with the treatment, antiangiogenesis for instance. With this hypothesis, we initially looked at a whole picture of mRNA expression with the f-NP treatment, aiming at the identification of target angiogenic factors that responded to the f-NP treatment. To do this, a quantitative PCR-array was used to analyze the gene expression of tumor tissues that were freshly removed from f-NP-treated human breast cancer (MCF-7) bearing nude mice. The results comprise Figure 2 and Supporting Information section S2. The results indicate that, a group of mRNA that encoded more than 10 angiogenic factors including Fgf1, Fgf6, Fgfr3; Cxcl1, Cxcl2, Cxcl5; Mmp19, Mmp2 and Mmp9; Lama5, and Tgfb1 and Tgfb2 were significantly downregulated after the f-NP treatment. Subsequently, we selectively verified the protein expression by Western blotting (Figure 2, inset).

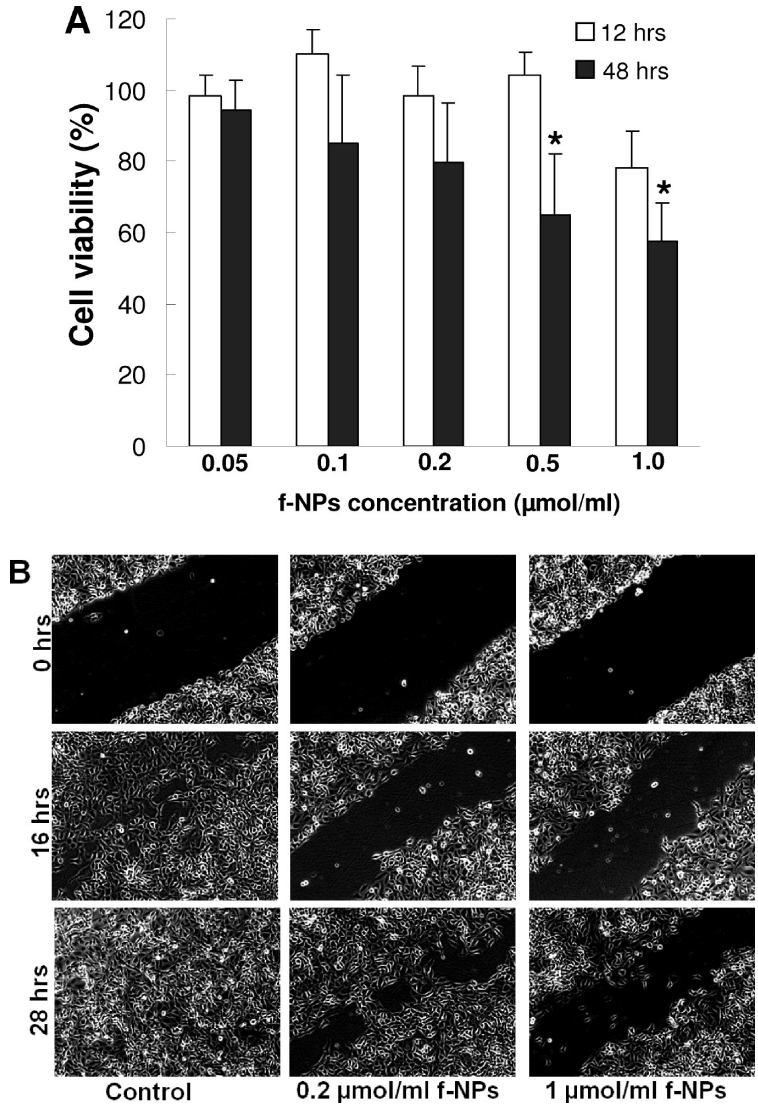

Figure 3. The *in vitro* angiogenesis assay of the f-NPs: (A) Cytotoxicity of the f-NPs on HMEC cells; (B) Inhibitory effect of cells migration when HMEC cells were treated by f-NPs at indicated time points.

Antiangiogenesis Activity of the f-NPs on Cellular Models. To validate our findings from the PCR-array, we initially studied cell viability and migration on human microvascular endothelial cells (HMEC) in the presence of the f-NPs. As shown in Figure 3A, the f-NPs dose-dependently inhibited the viability of HMEC cells. Cell viability was significantly inhibited when HMEC cells were treated by the f-NPs at a dose of >0.5 μmol/mL for 48 h. We also tested the effect of short-term incubations (12 h) with f-NPs on HMEC cells. The data showed no significantly inhibitory effect on cell viability after particle treatment even in the highest dose group, suggesting a time-dependent feature of inhibitory effect on the viability of endothelial cells. Figure 3B showed the inhibitory effect of cell migration after the NPs treatment on HMEC cells by a wound healing assay. In the control group, we observed that endothelial cells migrated and narrowed down the width of the gap as a function of time. This migration of HMEC cells was diminished when the cells were treated with f-NPs at a lower dose (0.2 μmol/mL), and >80% suppressed at a higher dose (1 μmol/mL) at all time points.

The cytotoxicity of the f-NPs on cancer cells and its dose−response are displayed in Supporting Information Figure S3. The cytotoxic anticancer drug paclitaxel[17] was used as a control. At a concentration of >0.1 μmol/mL, paclitaxel caused >90% inhibition of MCF-7 cell viability. In contrast with the severe cytotoxicity to cancer cells, the f-NPs had little effect on cell viability under the same conditions (Supporting Information Figure S3A). In the following apoptosis assay using

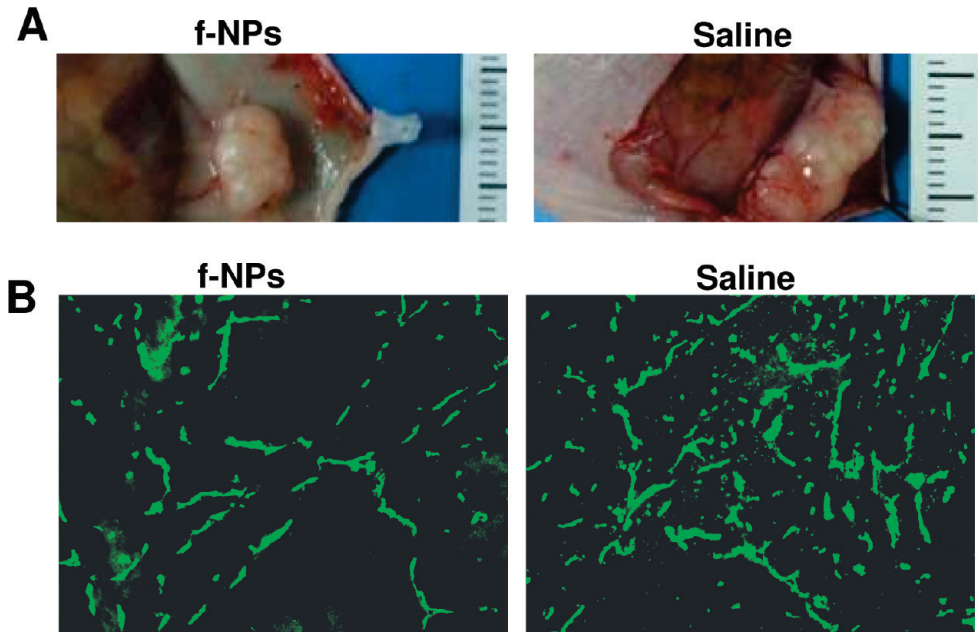

Figure 4. The *in vivo* antiangiogenesis effects of the f-NPs in mice. (A) Morphology of tumor tissue with the f-NPs or saline treatment. Less visible blood vessels can be found in the f-NP group. (B) The tumor tissues were stained for CD31 by immunohistochemistry. The f-NP treatment significantly reduced microvessel density (MVD) in tumor tissue compared to that of the control.

Annexin V-propidium iodide double staining, we clearly observed >80% percentage of necrotic (annexin V^+/PI^+) as well as apoptotic cells (annexin V^+/PI^-) after treatment with paclitaxel, however the f-NPs were incapable of inducing such effect (Supporting Information Figure S3B).

The f-NP Treatment Largely Reduced Tumor Microvessel Density in Tumor. We have already shown the PCR array result and those *in vitro* findings, the question that remained to be addressed was whether the antiangiogenesis activity could remain the same in an *in vivo* tumor model. In a MCF-7 human cancer xenograft model, an observation of tumor morphology provided visible evidence of the f-NPs induced antiangiogenesis activity *in vivo*, showing fewer visible blood vessels on the tumor surface of the particle-treated mice compare to the control (Figure 4A). Subsequently, a quantitative measurement of microvessel density (MVD) was performed in the tumor-bearing mice treated by the f-NPs and control using CD31 immunohistochemistry analysis. As shown in Figure 4B, MVD in tumors of the f-NP-treated mice was significantly reduced by >40% compared to control.

The f-NP Treatment Largely Reduced Tumor Blood Perfusion. We have shown that the f-NPs potently inhibited multiple angiogenic factors and resulted in a lower MVD *in vivo*. Logically, treatment using f-NPs is supposedly capable of reducing blood supply to tumor tissue, which eventually postpones or even stops tumor growth. To this end, we quantitatively analyzed the blood perfusion in tumor tissue at the end of 2 weeks treatment using dynamic contrast enhanced MRI (DCE-MRI) technique.[18,19] Hypothetically, it will show a rapid enhancement of signal intensity on the T1-weighted images after intravenous administration of Gd-DTPA (MRI contrast agent) if the tumor grows in a condition with sufficient blood supply; in contrast, a slower enhancement pattern can be found if a tumor is in a situation of poor blood perfusion. The reference images were captured before injection of Gd-DTPA in each group. Then, the mice in f-NP-, paclitaxel-, and saline-treated groups received Gd-DTPA injection through the tail vein, and their T1-weighted images were captured at the indicated time points. The image marked "1" in Figure 5A showed the pattern of the MRI signal intensity accumulated in tumor tissues before Gd-DTPA injection in the f-NP-treated mice. Images 2 (24 min) and 3 (42 min) are the results after Gd-DTPA injection in the f-NP-treated mice; those for the paclitaxel-treated mice are indicated in images 4−6, and for the saline-treated mice in images 7−9. We summarized the main findings from these image data in a point-to-point fashion as follows:

(1) Without f-NPs treatment, Gd-DTPA could easily enter into the tumor tissue (images 7−9), suggesting relatively sufficient blood supply was provided to the tumor tissue in control mice.

(2) The signal intensity in tumor tissues of f-NP-treated mice (the marked area in image 3) was significantly lower as compared to that in saline treated mice (image 9) or paclitaxel treated mice (image 6). This suggested that the f-NP treatment evidently decreased the blood perfusion into tumor tissues; otherwise, a bright MRI signal in tumor should be observed after Gd-DTPA injection.

(3) As f-NPs are known as a novel and efficient MRI contrast agent,[15,20−24] it would supposedly enhance

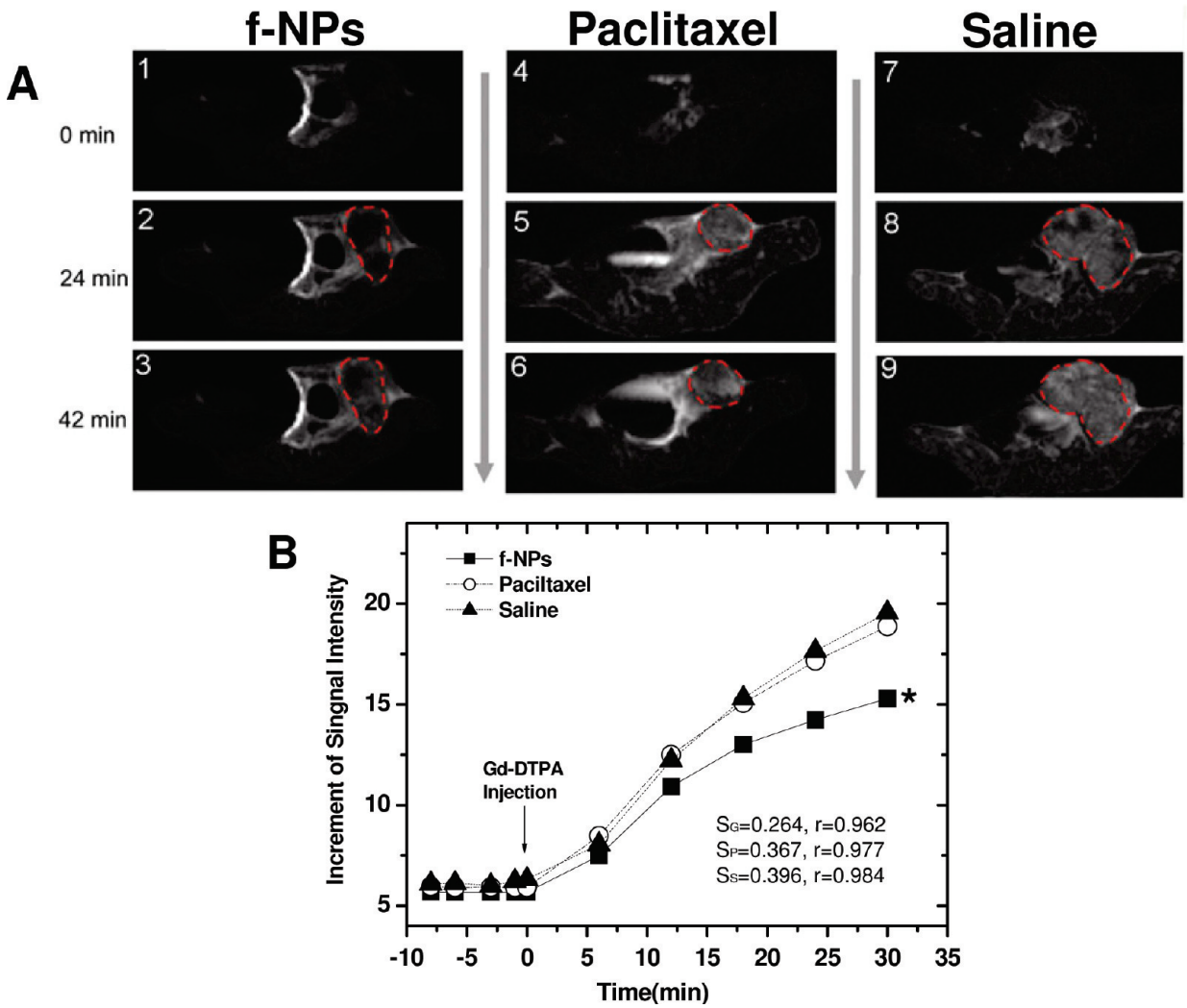

Figure 5. The f-NP treatment lowered blood perfusion to tumor tissues. (A) MRI images were captured after Gd-DTPA injection at indicated time points in f-NPs (1−3), paclitaxel- (4−6), and saline- (7−9) treated mice. The red circles indicate the boundary of the tumor tissues. (B) The semiquantitative analysis of MRI signal intensity in the f-NP-, paclitaxel- and saline-treated tumor mice. The slopes of f-NP-, paclitaxel- and saline-treated groups were marked as S_G, S_P, S_S, and respectively. The f-NP treatment efficiently depressed the speed of tumor blood supply compared to that of the control.

the T1-weighted signal when the mice received multiple
injections of f-NPs. Contrary to our expectation, the signal readout in f-NP-treated mice was even less intense than saline-treated mice. This inconsistency helps us gain an important sense: the bioaccumulation of Gd containing nanoparticles in the core area of a tumor, which is capable of enhancing MRI signal intensity, cannot compensate the signal debasement that is caused by the f-NPs induced poor blood perfusion.

We further quantitatively analyzed the dynamic blood supply to the core area of tumor tissues by performing linear regression of the signal intensities in the early stage after Gd-DTPA injection. The blood perfusion in the f-NP-treated mice gave an upslope of 0.264, but those in the paclitaxel- and saline-treated mice groups were 0.367 and 0.396, respectively (Figure 5B). This upslope directly reflected blood perfusion in tumor: the larger upslope indicates more blood was supplied to the tumor tissue per unit time.[18,19]

The f-NP Treatment Potently Inhibited Tumor Growth *in Vivo via* an Antiangiogenesis Mechanism without Interfering Normal Blood Vessel. The results above have shown that f-NPs can be used as a new and potent angiogenesis inhibitor. The next important thing we would like to know is whether f-NPs could provide good tumor inhibition *in vivo*. To this end, we performed animal experiments to verify the anticancer efficacy of the f-NP treatment. To compare the tumor inhibition rate and side effects with those of a commercially available drug, paclitaxel served as a control. Figure 6A showed the growth curve of human breast cancer in different mice groups treated with f-NPs, paclitaxel, or saline, respectively. On the basis of the tumor size calculation, f-NP treatment at 3.8 mg/kg dose showed a comparable tumor inhibition capability to that

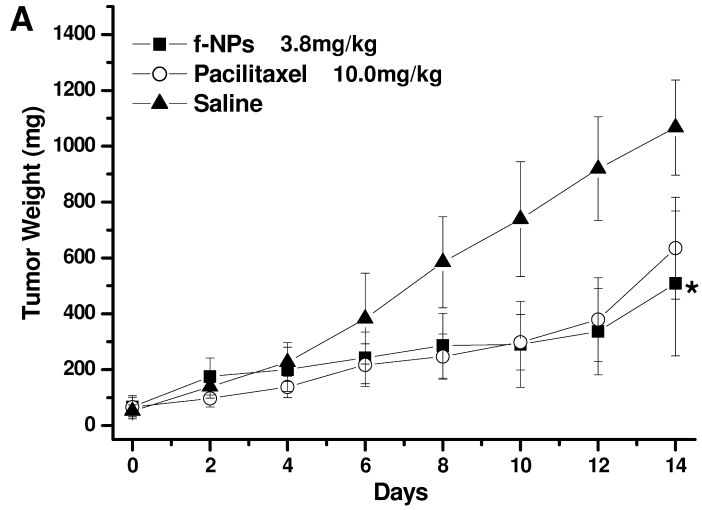

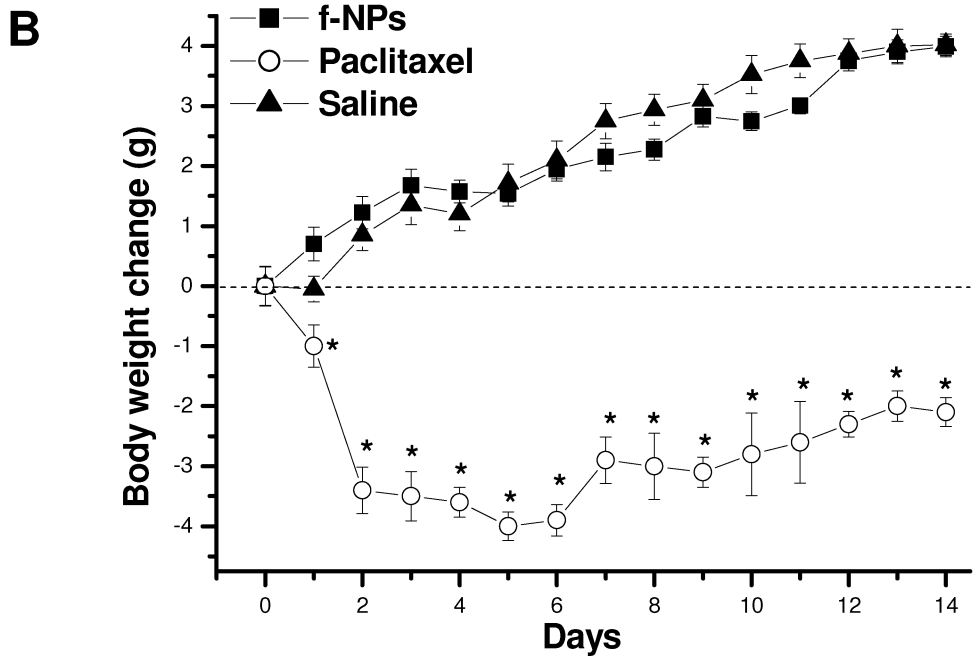

C

Treatment	ALT (IU/L)	TBA (μmol/L)	BUN (mmol/L)	Cr (μmol/L)
f-NPs	80.3±24.4[a,b]	3.9±2.5	10.7±2.8	54.2±5.7
Paclitaxel	184.2±45.1	3.0±1.2	10.1±2.0	54.1±4.2
Saline	198.8±77.7	2.8±0.3	9.1±2.7	54.3±6.6
Normal nude mice	36.5±4.9	2.4±0.4	10.5±1.0	55.7±2.5

Figure 6. The f-NPs potently inhibited tumor growth without detectable side effecs. (A) Tumor growth curves in f-NP- (■), paclitaxel- (○), and saline- (▲) treated mice are shown. (B) The figure shows body weight changes along with different treatments. The dotted line indicated no body weight change. (*) $p < 0.05$. (C) Blood chemistry assay of the mice with different treatments. (a) $p < 0.05$ compare to saline control; (b) $p < 0.05$ compare to paclitaxel.

of a 10 mg/kg mass dose of paclitaxel. In spite of the one-third dosage used in the treatment, the f-NPs gave an even slightly higher tumor inhibition rate (48.8% on average) *versus* paclitaxel (45.1% on average) which is considered as the breast cancer-specific chemotherapeutic agent in clinic. At the end point of the experiment, the tumor weight of paclitaxel-treated mice was ~15% larger than that of the f-NPs treated mice.

Regarding the nanotoxicity issue of this particle, a series of toxicity evaluations were performed along

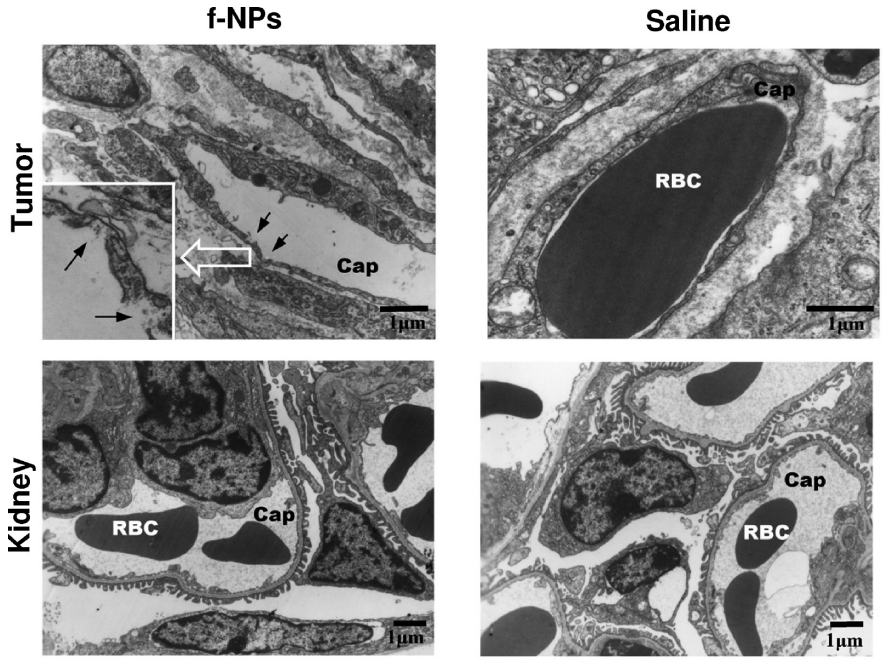

Figure 7. Electron microscopy to determine the ultrastructural changes in tumor blood vessel and normal blood vessel. The f-NPs further damaged the integrity of tumor vessels, but showed limited effects on normal blood vessels in kidneys. "Cap" indicates the capillary vessel, and "RBC" denotes red blood cells.

with the treatment. We did not observe pronounced side effects during or at the end of treatment in nanoparticle-treated mice. No animals died in f-NP-treated group, while during the treatment one and two animals died in paclitaxel- and saline-treated groups, respectively. Paclitaxel treatment significantly decreased mice body weight, in contrast, the mice receiving continuously f-NPs treatment did not show body weight loss compared to control (Figure 6B). We also surveyed the alteration of blood biochemical parameters, including total bile acid (TBA), alanine aminotransferase (ALT), blood urea nitrogen (BUN), and creatinine (Cr). Their alterations reflect the damages of renal and hepatic functions (Figure 6C). Tumor-bearing mice showed elevated ALT and TBA levels *versus* normal nude mice, indicating that tumor growth itself heavily damaged the renal and hepatic function. Interestingly, the f-NP treatment was able to decrease the tumor induced elevated ALT level from 198.8 ± 77.7 (IU/L) to 80.3 ± 24.4 (IU/L). No such favorable function was found in paclitaxel-treated mice group. In the f-NP-treated mice, necropsy and pathological examinations did not show observable pathological changes, but the paclitaxel-treatment induced irreversible glomerulitis in kidney and cell necrosis in splenic units (Supporting Information Figure S4).

Another key question that needs to be clarified is whether the f-NP treatment could affect lesions on normal blood vessels. Using TEM techniques, we directly observed changes in the capillary vessels in tumor stroma after f-NP treatment. The f-NP treatment further damaged the integrity of tumor vessels; disfigurements or breaches in the cell layer can be easily identified (Figure 7, upper panel). Curiously, the capillary vessels in normal tissue (e.g., kidney) showed no changes with or without f-NP treatment (Figure 7, lower panel). No pronounced abnormalities such as gaps, disfigurements, or breaches in the cell layer of blood vessels in normal organs were observed.

DISCUSSION

In this paper, we show the possibility of using the $Gd@C_{82}(OH)_{22}$ nanoparticles as a potent anticancer drug and reveal a new category of angiogenesis inhibitor that is in a "particulate" form, capable of showing more favorable uniqueness than the "molecular" form of traditional anticancer medicines. In the mRNA level, the f-NPs significantly downregulated a group of genes that encoded more than 10 angiogenic factors including Fgf1, Fgf6, Fgfr3; Cxcl1, Cxcl2, Cxcl5; Mmp19, Mmp2, Mmp9; Lama5, and Tgfb1 and Tgfb2. These were then selectively verified at the protein level. In cellular experiments, the f-NPs dose-dependently inhibited cell viability and migration ability of human microvascular endothelial cells. This was directly confirmed by a morphology observation showing fewer visible blood vessels on the tumor surface after the f-NP treatment. A quantitative analysis indicated that MVD in tumors of f-NP treated mice was reduced by >40% compared to control. With the assistance of MRI, we further found that the tumor vascular system was well established in the control mice, allowing Gd-DTPA molecules easily pass through the blood vessels and enter into the tumor tissue. In contrast, after the f-NP treatment, tumor blood perfusion was evidently decreased. The bioaccumulation of Gd containing nanoparticles in the core

area of the tumor could not compensate the T1-weighted signal debasement which was caused by the f-NPs induced low MVD, resulting in insufficient blood perfusion. A treatment using 3.8 mg/kg dose of f-NPs yields a comparable therapeutic effect to the paclitaxel treatment at a dose of 10 mg/kg. In spite of the one-third dosage used in the treatment, the f-NPs gave a slightly higher tumor inhibition rate *versus* paclitaxel which is considered as the first-line drug in breast cancer treatment. In addition, we found that the tumor-impaired hepatic and renal function could be partially restored with the f-NP treatment, but no such favorable effect was found in paclitaxel-treated mice. Moreover, the f-NP treatment showed little toxicity and side effects, while the cytotoxic anticancer drug exerted grave side effects, including body weight loss and pathological abnormalities in the kidney and spleen.

This work has attempted to explore a new category of angiogenesis inhibitor of "particulate" form by surface-functionalized fullerene nanoparticles. The f-NPs showed much more favorable uniqueness than the "molecular" form of conventional anticancer medicine, such as high biocompatibility, good stability, low toxicity, and potent inhibition efficacy on multiple angiogenic factors. Key advantages of this pharmaceutically active carbon-nanomaterial include the following: (1) Unlike traditional angiogenesis inhibitor in "molecular" form, a huge particle surface area can be chemically modified with functional groups, which might be the origin for yielding simultaneous inhibition effects on a wide spectrum of more than 10 angiogenic factors. Individually blocking those factors (*e.g.*, VEGF,[5] Cxcl1,[25] and FGF6[26]) has been shown as a potential approach in cancer therapy because of the key roles of those angiogenic factors in the signal cascade. The wide spectrum inhibition of multiple factors that traditional inhibitors do not possess highlights the advantage of the f-NPs in nanoparticle form. This nature is also beneficial for overcoming drug resistance, because single inhibition can select for tumor cells that overexpress other angiogenic factors.[7] (2) Since the display of endothelial cells in tumor blood vessels are not smooth and well organized like in normal blood vessels, tumor blood vessels become more chaotic, disorganized, and leaky.[1,2] Well controlled size in the nano range allowed the particles to passively accumulate in the solid tumor surface *via* an enhanced permeability retention (EPR) effect.[27,28] This can help us understand why the f-NPs significantly interfere with tumor blood vessels while having little effect on normal blood vessels. (3) The inhibition of tumor angiogenesis has been verified as a low toxic type of anticancer therapy,[29] as is the case with f-NP treatment. High biocompatibility endows the particles with a wide tolerance window that traditional cytotoxic anticancer drugs do not have. This feature allows long-term treatment using a relatively high dose without exerting pronounced toxicity. (4) Since the paramagnetic f-NPs were also designed as a new generation of MRI contrast agent,[15,20−24] it may be applied to not only cancer therapy but also cancer diagnosis to simultaneously monitor tumor death along with the treatment in clinic. (5) With the assistance of high-content or high-rapid screening technologies (*e.g.*, PCR-array, molecular simulation), we realized that multiple mechanisms may simultaneously be involved in the anticancer process, thus yielding a high anticancer efficacy *via* a combinatory or synergistic effect. Though it is not possible at this stage to explicitly summarize comprehensive anticancer mechanisms of the f-NPs, those additional mechanisms at least include oxidative stress regulation,[30] scavenging of free radicals,[31] and immunomodulatory effects.[32,33]

The ideal paradigm of exploring the biomedical activity of nanomaterials, including pharmaceutical activity as well as nanotoxicity, is to establish the link between physicochemical properties and biobehaviors using the knowledge of quantitative structure activity relationships (QSAR) that generated in the nano-bio interface.[34] In the practice of exploring the biobehaviors of the f-NPs, we realize that some essential physicochemical properties of the f-NPs directly determine the anticancer activity.

First, the encaged metallic atom plays an important role in its potent anticancer activities. In a pristine Gd@C_{82} molecule, because of the electron donation from the Gd atom, the highest occupied molecular orbital (HOMO) distributes mainly on the opposite side of the C_{82} cage compared to the Gd location,[35] which directly influences local distributions of outer chemical groups which are hydroxyls in the present study. In the case using a surface-modified carbon cage without a metallic atom, we only found a slight inhibitory rate of cancer growth, much lower than the case with the Gd encaged. This is probably due to modulation of the electronic or charge state of the cage surface caused by inserting the metallic atom into the cage.[36−39] This indicates that the surface charge is an essential factor that influences the interaction between nanomaterial and biological system.

Second, in the f-NPs, the hydroxyl groups are asymmetrically distributed on the Gd@C_{82} cage due to the localized HOMO distribution.[37] On one side of the nanocage, OH groups serve as the electron donor, which enhances the local intensity of electronic interactions with the target biomolecules. On the opposite side of the carbon cage, the less charge density leads −OH groups to serve as electronic acceptors.[35,37] Our recent experiment suggested that the local distribution of hydroxyls on the surface of Gd@C_{82} led to the splitting of the innermost metallic Gd atoms at the 5p level.[37] Accordingly, the f-NPs exhibit both the hydrophilic and hydrophobic features, depending on the different cage positions to which the biomolecules may approach. In addition, we are currently working on the comparison

of different surface modifications, including −OH, −COOH, $-NH_2$, and −SH, aiming for understanding of the role of surface modification in this system.

Third, since the carbon cage isolates the Gd atom, the toxicity of heavy ions is completely avoided. Undoubtedly, this is an advantageous feature for the f-NPs, showing high anticancer efficacy with low side-effects *in vivo* (Figure 6).

With the assistance of molecular simulation, these important links between physicochemical properties and bioactivity are being established in our lab, allowing us to gain more sense in terms of the rational design of carbon-based nanomaterials with the desired bioactivity. The "design" experiments are intensively carried out in place of random attempts to study the bioapplication of metallofullerene-based nanomaterials.

CONCLUSION

We show the capability of using $Gd@C_{82}(OH)_{22}$ nanoparticles (f-NPs) directly as a novel anticancer drug, and reveal a new category of potent angiogenesis inhibitor that is in "particulate form" which shows more favorable uniqueness than the "molecular form" of traditional anticancer medicines. Superior to the traditional molecular medicine, these findings provide new insights for developing a new form of medicine, namely particulate medicine, in cancer therapy.

MATERIALS AND METHODS

Preparation of $Gd@C_{82}(OH)_{22}$ Nanoparticles (f-NPs). The gadolinium metallofullerenes ($Gd@C_{82}$) were synthesized by an arc-discharge method using the composite rods consisting of Gd_2O_3 (purity >99.99%) and graphite (purity >99.99%) in a He atmosphere. The $Gd@C_{82}$ was separated by a two-step high performance liquid chromatography (HPLC, LC908-C60, Japan Analytical Industry Co) technique with Φ 20 mm × 250 mm 5PBB columns (Nacalai Co, Japan) and then Φ 20 mm × 250 mm Buckyprep columns (Nacalai Co., Japan). The purity of the final $Gd@C_{82}$ product was greater than 99.5%. $Gd@C_{82}(OH)_{22}$ was synthesized by the alkaline reaction.[36−39] Briefly, $Gd@C_{82}$ toluene solution was first mixed with an aqueous solution containing 50% NaOH. Several drops of 40% TBAH (tetrabutylammonium hydroxide) were added into the reaction system as catalyst. After vigorous stirring at room temperature, brown color sediment appeared on the bottom of the beaker, meanwhile toluene solution became basically colorless. To remove the remnants of TBAH and NaOH, a thorough washing process was performed by water and MeOH. Then, the sediment was dissolved into deionized water with continuous stirring for 24 h until the solution color became clearly reddish brown. Finally, the solution was purified by a Sephadex G-25 column chromatography (5 × 50 cm^2) with an eluent of distilled water. The synthesized material is a mix of products including $Gd@C_{82}(OH)_x$ with a broad *x* distribution from 2 to more than 40 hydroxyls groups. Because many structural isomers coexist in the solution, we have to obtain a $Gd@C_{82}(OH)_x$ formulation with a narrow range of hydroxyl number distribution. A very long column was used, and the needed fraction (eluate) was collected in a time interval of 2 min. The molecule weight was determined by elemental analysis method, MALDI-TOF-MS technique (AutoFlex, Bruker Co., Germany), and X-ray photoemission spectroscopy (XPS, Beijing Synchrotron Radiation Facility). The narrowest range of hydroxyl number of $Gd@C_{82}(OH)_x$ that we obtained was four hydroxyls: $Gd@C_{82}(OH)_{20-24}$ (referred to as $Gd@C_{82}(OH)_{22}$ for short). The dry $Gd@C_{82}(OH)_{22}$ powder was accurately weighed and freshly dissolved in 0.9% sterile saline solution for further anticancer experiments.

Physicochemical Characterization of the f-NPs. The f-NPs were characterized for size, zeta potential, and shape. The morphology was characterized using a scanning electron microscope (SEM) at a concentration of 50 μg/mL. The zeta potential in saline (25 μg/mL) with a series of pH values ranging from 3 to 8 were measured by ZetaSizer Nano (Malvern Instruments Ltd., Worcestershire, U.K.).

Cell Culture and Cytotoxicity Assay. The MCF-7 cells were cultured in RPMI 1640 medium (Gibco Inc., Rockville, MD) supplemented with 10% FBS with 100 U/mL penicillin, and 100 μg/mL streptomycin in humidified incubation with 5% CO_2. HMEC cells were grown in MCDB-131 medium supplemented with 15% FBS, 2 mM L-glutamine, and 10 ng/mL epidermal growth factor. A cytotoxicity assay was performed with a Cell Counting Kit-8 (CCK-8, Dojindo Laboratories, Japan). The cells were placed into 96-well culture plates with flat bottoms (Corning Inc., Corning, NY) at a concentration of 1 × 10^5 cells/well. The cells were treated with the f-NPs in a series of concentrations for indicated times. PBS was set as control (considered as 100% cell viability). After incubation, 10 μL of CCK-8 solution were added, and the plates were incubated for an additional 1−3 h. We also assessed the induction of apoptosis and necrosis at 48 h through the use of Annexin V/PI staining on MCF-7 cells. Briefly, 5 × 10^5 cells were harvested and stained by Annexin V-PI working solution (Trevigen). The flow cytometry assay was performed on a FACScan machine (BD Biosciences). Data analysis was performed by BD CellQuest sofeware.

Cell Migration Assay. Migration activity was tested using a previously described method.[40] Briefly, HMEC cells were seeded into a 24-wells plate at a concentration of 4 × 10^5 cells/mL and cultured overnight as described in the cell culture section. Then, the cells were scraped with a line in the middle of the well by a sterile peptide tip, resulting in a wound with a width of ~0.2 mm. After being washed with phosphate-buffered saline (PBS) for three times, new medium was added into the wells with or without f-NPs at the desired concentration. The microscope images were captured at indicated time points.

Animals and Tumor Model. Athymic BALB/c nu/nu female mice (weighing 16.0 ± 1.0 g) were purchased from the Cancer Institute and Cancer Hospital, Chinese Academy of Medical Sciences, and maintained under specific pathogen-free (SPF) conditions. Nude mice were acclimated in the controlled environment (22 ± 1 °C in temperature, 60 ± 10% in humidity, and a 12 h light/dark cycle) with free access to sterile distilled water and commercial laboratory complete food containing no pathogens. All animal experiments were performed in compliance with local ethics committee guidelines. The human breast cancer MCF-7 cell line was provided by the Cancer Institute and Cancer Hospital, Chinese Academy of Medical Sciences. The tumor cell suspension (0.2 mL, 1 × 10^7cells/mL) was injected subcutaneously into four nude mice. Twenty days after the injection, the mice were sacrificed (tumor were about 1.2 cm in diameter), and the subcutaneous tumor was divided into small pieces (each measuring approximately 1−2 mm^3). The small tumor tissues were then subcutaneously inoculated into the left inguinal region of the ether-anesthetized nude mice, using a trocar needle. 17β-Estradiol dipropionate at 5 mg/kg and 17α-progesterone caproate at 250 mg/kg were injected intramuscularly into mice bearing MCF-7 on the day of tumor inoculation to ensure exponential tumor growth. The tumors were measured (length and width) with sliding calipers three times weekly by the same observer.

Animal Experiments. The animals were used 1 week after tumor implantation. The tumor bearing nude mice were randomly divided into three groups, 12 in each group. In the experimental group, the mice were intraperitoneally (i.p.) administered $Gd@C_{82}(OH)_{22}$ saline solution once a day at the dose of 2.5 μmol/kg (3.8 mg/kg), after the tumor tissue implantation into

the animal for 7 days, continuing until the mice were sacrificed. Paclitaxel was used as the control. Paclitaxel was given four times at intervals of 3 days at the dose of 10 mg/kg. When the paclitaxel was not injected, saline solution was injected instead of it. A 0.9% saline solution was used as a negative control in the anticancer experiment. The daily administration process lasted 14 days. The body weight and tumor size were used as two basic parameters in the experiments, and tumor growth curve and body weight change were prepared as a function of time. Tumor weight was calculated according to the formula: tumor weight (mg) = length (mm) × (width (mm))^2/2.[41]

Angiogenesis PCR-Array. Total RNA was isolated using Trizol according to the manufacturer's instructions (Invitrogen Inc., Carlsbad, CA). Genomic DNA contamination was eliminated by Dnase treatment by using a Rneasy Micro Kit (Qiagen GmbH, Hilden, Germany), and yield and quality of RNA was tested by denaturing ararose gel electrophoresis before starting PCR-Array. Mouse Angiogenesis RT^2 Profiler PCR Array (APMM-024) and RT^2 Real-Timer SyBR Green/ROX PCR Mix were purchased from SuperArray Bioscience Corporation (Frederick, MD). PCR was performed on an Applied Biosystems 7500 and 7500 Fast Real-Time PCR Systems. The data analysis was performed by the program provided by Supperarray (http://www.superarray.com/rt_pcr_product/HTML/APMM-024A.html). Briefly, the △△Ct method was used. For each, gene fold-changes were calculated as the difference in gene expression between the nanoparticle treatment group and the saline control. A positive value indicates gene up-regulation and a negative value indicates gene down-regulation.

Magnetic Resonance Imaging (MRI). Tumor-bearing mice from the f-NP, paclitaxel, and saline groups were anesthetized by urethane at a dose of 500 mg/kg and intravenously injected with gadopentetic acid dimeglumine salt solution (Gd-DTPA, Schering Pharmaceutical Company, Berlin, Germany) at a dose of 1.5 mmol/kg. Tumor images were obtained on a 4.7T Bruker Biospec 47/30 MRI imager at 37 °C. Axial images were acquired with 500 ms/15 ms (repetition/echo), and four signals were collected by multislice and multiecho techniques. A series of T_1-weighted images of tumor tissue were obtained before and after intravenous injection of Gd-DTPA. In all of the experiments, imaging was monitored up to 45 min post-Gd-DTPA injection at intervals of 6 min. After standardization of the signal intensities to that of the phantom, the signal intensity of the tumor region was calculated by Paravision, Bruker (Bruker Co., Germany).

Immunohistochemistry. O.C.T-embedded tumor tissues of experimental mice were sectioned at 5 μm, and the slices were washed three times with PBS. Frozen slides are fixed by cold acetone for 15 min. Afterward, the slides were incubated in 3% hydrogen peroxide in methanol for 30 min and 1% normal goat serum at room temperature for 12 min. Then the slides were incubated with rat-antimouse CD31 monoclonal antibody (diluted with PBS, BD Bioscience, USA) at 4 °C overnight. On the following day, the primary antibody was removed and washed with PBS for 3 times, FITC-labeled goat-antirat IgG (Zhongshan Biocompany, China) was then added. The images were taken by fluorescence microscope (Olympus X71, Japan).

Western Blotting. To determine the protein expression of VEGF and FGF, Western blotting was performed. A 200 μg portion of each precleared, detergent-solubilized tumor tissue was used for total protein preparation. After separation by SDS gel electrophoresis, samples were transferred to nylon membranes and incubated with primary antibodies (Santa Cruz Sc-7269 and BD Biosciences 610072) followed by fluorescence-conjugated antimouse secondary antibodies (Amersham Pharmacia, Piscataway, NJ).

Pathological Examination. Once the tested mice were sacrificed at the end point of the experiments, the organs including the heart, liver, spleen, lung, kidney, stomach, brain, and tumor were removed and accurately weighed. Some of them were sent for pathological examination.

Transmission Electron Microscopy (TEM). Standard TEM ultrastructural analyses were performed. Ultrathin (60−80 nm) tumor sections were examined under a Philips CM120 electron microscope at 60 kV using a systematic-random sampling routine. Capillary morphology, including red blood cells (RBC), and their relationship to endothelial cells were evaluated in more detail in the f-NPs and saline groups. The spatial relationships between capillaries and endothelial cells and capillary integrity were determined. The gaps in the lumen of capillaries were carefully identified and recognized as an index to assess capillary integrity. Similarly, the ultrastructural analyses of normal blood vessels were performed.

Statistical Analysis. All of the results were calculated as mean ± standard deviation (SD). The statistical significance of the changes between tested groups and the control group were analyzed by the multiple comparison test method (*t* test) using SAS 6.12 (SAS Institute, Inc., Cary, NC).

Acknowledgment. The authors are grateful for the support of the MOST 973 program (2006CB705601, 2009CB930204, 2010CB933904), NSFC (10525524), and CAS Knowledge Innovation Program.

Supporting Information Available: Additional characterization data of the f-NPs; effects of the f-NPs on the mRNA level of MCF-7 breast carcinoma in nude mice; cytotoxicity of the f-NPs on MCF-7 cancer cells; pathology examination of tumor bearing mice treated by the f-NPs, paclitaxel, and saline. This material is available free of charge *via* the Internet at http://pubs.acs.org.

REFERENCES AND NOTES

1. Folkman, J. Angiogenesis. *Annu. Rev. Med.* **2006**, *57*, 1–18.
2. Carmeliet, P.; Jain, R. K. Angiogenesis in Cancer and Other Diseases. *Nature* **2000**, *407*, 249–257.
3. Kerbel, R. S. Antiangiogenic Therapy: A Universal Chemosensitization Strategy for Cancer. *Science* **2006**, *312*, 1171–1175.
4. Mendel, D. B.; Schreck, R. E.; West, D. C.; Li, G.; Strawn, L. M.; Tanciongco, S. S.; Vasile, S.; Shawver, L. K.; Cherrington, J. M. The Angiogenesis Inhibitor SU5416 Has Long-Lasting Effects on Vascular Endothelial Growth Factor Receptor Phosphorylation and Function. *Clin. Cancer Res.* **2000**, *6*, 4848–4858.
5. Folkman, J. Antiangiogenesis in Cancer Therapy-Endostatin and Its Mechanisms of Action. *Exp. Cell Res.* **2006**, *312*, 594–607.
6. Ferrara, N.; Hillan, K. J.; Gerber, H.-P.; Novotny, W. Discovery and Development of Bevacizumab, An Anti-VEGF Antibody for Treating Cancer. *Nat. Rev. Drug Discovery* **2004**, *3*, 391–400.
7. McCarty, M. F.; Liu, W.; Fan, F.; Parikh, A.; Reimuth, N.; Stoeltzing, O.; Ellis, L. M. Promises and Pitfalls of Anti-angiogenic Therapy in Clinical Trials. *Trends Mol. Med.* **2003**, *9*, 53–58.
8. Katanasaka, Y.; Ida, T.; Asai, T.; Maeda, N.; Oku, N. Effective Delivery of an Angiogenesis Inhibitor by Neovessel-Targeted Liposomes. *Int. J. Pharm.* **2008**, *360*, 219–224.
9. Ferrari, M. Cancer Nanotechnology: Opportunities and Challenges. *Nat. Rev. Cancer* **2005**, *5*, 161–171.
10. Farokhzad, O. C.; Langer, R. Impact of Nanotechnology on Drug Delivery. *ACS Nano* **2009**, *3*, 16–20.
11. Wang, M. D.; Shin, D. M.; Simons, J. W.; Nie, S. Nanotechnology for Targeted Cancer Therapy. *Expert Rev. Anticancer Ther.* **2007**, *7*, 833–837.
12. Nel, A. E.; Madler, L.; Velegol, D.; Xia, T.; Hoek, E. M. V.; Somasundaran, P.; Klaessig, F.; Castranova, V.; Thompson, M. Understanding Biophysicochemical Interactions at the Nano−Bio Interface. *Nat. Mater.* **2009**, *8*, 543–557.
13. *Cancer Nanotechnology Plan: A Strategic Initiative to Transform Clinical Oncology and Basic Research Through the Directed Application of Nanotechnology*; National Cancer Institute, National Institutes of Health: Washington, DC, 2004.
14. Cagle, D. W.; Kennel, S. J.; Mirzadeh, S.; Alford, J. M.; Wilson, L. J. *In Vivo* Studies of Fullerene-Based Materials Using Endohedral Metallofullerene Radiotracers. *Proc. Natl. Acad. Sci. U.S.A.* **1999**, *96*, 5182–5187.
15. Xing, G.; Yuan, H.; He, R.; Gao, X.; Jing, L.; Zhao, F.; Chai, Z.; Zhao, Y. The Strong MRI Relaxivity of Paramagnetic Nanoparticles. *J. Phys. Chem. B* **2008**, *112*, 6288–6291.

16. Chen, C.; Xing, G.; Wang, J.; Zhao, Y.; Li, B.; Tang, J.; Jia, G.; Wang, T.; Sun, J.; Xing, L.; Yuan, H.; Gao, Y.; Meng, H.; Chen, Z.; Zhao, F.; Chai, Z.; Fang, X. Multihydroxylated $[Gd@C_{82}(OH)_{22}]_n$ Nanoparticles: Antineoplastic Activity of High Efficiency and Low Toxicity. *Nano Lett.* **2005**, *5*, 2050–2057.
17. Guolin, T.; Li, H.; Chen, J.; Jiang, M.; Ma, Y.; Liu, X.; Sun, H.; Guiyuan, L. Apoptosis Induced by Low-Dose Paclitaxel Is Associated with p53 Upregulation in Nasopharyngeal Carcinoma Cells. *Int. J. Cancer* **2002**, *97*, 168–172.
18. Padhani, A. R. MRI for Assessing Antivascular Cancer Treatments. *Br. J. Radiol.* **2003**, *76*, S60–80.
19. Tofts, P. S.; Berkowitz, B.; Schnall, M. D. Quantitative Analysis of Dynamic Gd-DTPA Enhancement in Breast Tumors Using a Permeability Model. *Magn. Reson. Med.* **1995**, *33*, 564–568.
20. Kato, H.; Kanazawa, Y.; Okumura, M.; Taninaka, A.; Yokawa, T.; Shinohara, H. Lanthanoid Endohedral Metallofullerenols for MRI Contrast Agents. *J. Am. Chem. Soc.* **2003**, *125*, 4391–4397.
21. Laus, S.; Sitharaman, B.; Toth, E.; Bolskar, R. D.; Helm, L.; Asokan, S.; Wong, M. S.; Wilson, L. J.; Merbach, A. E. Destroying Gadofullerene Aggregates by Salt Addition in Aqueous Solution of $Gd@C_{60}(OH)_x$ and $Gd@C_{60}[C(COOH_2)]_{10}$. *J. Am. Chem. Soc.* **2005**, *127*, 9368–9369.
22. Bolskar, R. D.; Benedetto, A. F.; Husebo, L. O.; Price, R. E.; Jackson, E. F.; Wallace, S.; Wilson, L. J.; Alford, J. M. First Soluble $M@C_{60}$ Derivatives Provide Enhanced Access to Metallofullerenes and Permit *in Vivo* Evaluation of $Gd@C_{60}[C(COOH)_2]_{10}$ as a MRI Contrast Agent. *J. Am. Chem. Soc.* **2003**, *125*, 5471–5478.
23. Mikawa, M.; Kato, H.; Okumura, M.; Narazaki, M.; Kanazawa, Y.; Miwa, N.; Shinohara, H. Paramagnetic Water-Soluble Metallofullerenes Having the Highest Relaxivity for MRI Contrast Agents. *Bioconjugate Chem.* **2001**, *12*, 510–514.
24. Sitharaman, B.; Bolskar, R. D.; Rusakova, I.; Wilson, L. J. $Gd@C_{60}[C(COOH)_2]_{10}$ and $Gd@C_{60}(OH)_x$: Nanoscale Aggregation Studies of Two Metallofullerene MRI Contrast Agents in Aqueous Solution. *Nano Lett.* **2004**, *4*, 2373–2378.
25. Wang, D.; Wang, H.; Brown, J.; Daikoku, T.; Ning, W.; Shi, Q.; Richmond, A.; Strieter, R.; Dey, S. K.; DuBois, R. N. CXCL1 Induced by Prostaglandin E2 Promotes Angiogenesis in Colorectal Cancer. *J. Exp. Med.* **2006**, *203*, 941–951.
26. Ropiquet, F.; Giri, D.; Kwabi-Addo, B.; Mansukhani, A.; Ittmann, M. Increased Expression of Fibroblast Growth Factor 6 in Human Prostatic Intraepithelial Neoplasia and Prostate Cancer. *Cancer Res.* **2000**, *60*, 4245–4250.
27. Matsumura, Y.; Maeda, H. A New Concept for Macromolecular Therapeutics in Cancer Chemotherapy: Mechanism of Tumoritropic Accumulation of Proteins and the Antitumor Agent SMANCS. *Cancer Res.* **1986**, *46*, 6387–6392.
28. Nie, S.; Xing, Y.; Kim, G. J.; Simons, J. W. Nanotechnology Applications in Cancer. *Annu. Rev. Biomed. Eng.* **2007**, *9*, 12.112.32.
29. O'Reilly, M. S.; Boehm, T.; Shing, Y.; Fukai, N.; Vasios, G.; Lane, W. S.; Flynn, E.; Birkhead, J. R.; Olsen, B. R.; Folkman, J. Endostatin: An Endogenous Inhibitor of Angiogenesis and Tumor Growth. *Cell* **1997**, *88*, 277–285.
30. Wang, J.; Chen, C.; Li, B.; Yu, H.; Zhao, Y.; Sun, J.; Li, Y.; Xing, G.; Yuan, H.; Tang, J.; *et al*. Antioxidative Function and Biodistribution of $[Gd@C_{82}(OH)_{22}]_n$ Nanoparticles in Tumor-Bearing Mice. *Biochem. Pharmacol.* **2006**, *71*, 872–881.
31. Yin, J.-J.; Lao, F.; Meng, J.; Fu, P. P.; Zhao, Y.; Xing, G.; Gao, X.; Sun, B.; Wang, P. C.; Chen, C.; Liang, X.-J. Inhibition of Tumor Growth by Endohedral Metallofullerenol Nanoparticles Optimized as Reactive Oxygen Species Scavenger. *Mol. Pharmacol.* **2008**, *74*, 1132–1140.
32. Liu, Y.; Jiao, F.; Qiu, Y.; Li, W.; Lao, F.; Zhou, G.; Sun, B.; Xing, G.; Dong, J.; Zhao, Y.; *et al*. The effect of $Gd@C_{82}(OH)_{22}$ Nanoparticles on the Release of Th1/Th2 Cytokines and Induction of TNF-[α] Mediated Cellular Immunity. *Biomaterials* **2009**, *30*, 3934–3945.
33. Yang, D.; Zhao, Y.; Guo, H.; Li, Y.; Tewary, P.; Xing, G.; Hou, W.; Oppenheim, J. J.; Zhang, N. $[Gd@C_e(OH)_{22}]_n$ Nanoparticles Induce Dendritic Cell Maturation and Activate Th1 Immune Responses. *ACS Nano* **2010**, *4*, 1178–1186.
34. Meng, H.; Xia, T.; George, S.; Nel, A. E. A Predictive Toxicological Paradigm for the Safety Assessment of Nanomaterials. *ACS Nano* **2009**, *3*, 1620–1627.
35. Senapati, L.; Schrier, J.; Whaley, K. B. Electronic Transport, Structure, and Energetics of Endohedral Gd@C82 Metallofullerenes. *Nano Lett.* **2004**, *4*, 2073–2078.
36. Tang, J.; Xing, G.; Yuan, H.; Cao, W.; Jing, L.; Gao, X.; Qu, L.; Cheng, Y.; Ye, C.; Zhao, Y.; *et al*. Tuning Electronic Properties of Metallic Atom in Bondage to a Nanospace. *J. Phys. Chem. B* **2005**, *109*, 8779–8785.
37. Tang, J.; Xing, G.; Zhao, Y.; Jing, L.; Gao, X.; Cheng, Y.; Yuan, H.; Zhao, F.; Chen, Z.; Meng, H.; *et al*. Periodical Variation of Electronic Properties in Polyhydroxylated Metallofullerene Materials. *Adv. Mater.* **2006**, *18*, 1458–1462.
38. Tang, J.; Xing, G.; Zhao, F.; Yuan, H.; Zhao, Y. Modulation of Structural and Electronic Properties of Fullerene and Metallofullerenes by Surface Chemical Modifications. *J. Nanosci. Nanotechnol.* **2007**, *7*, 1085–1101.
39. Qu, L.; Cao, W.; Xing, G.; Zhang, J.; Yuan, H.; Tang, J.; Cheng, Y.; Zhang, B.; Zhao, Y.; Lei, H. Study of Rare Earth Encapsulated Carbon Nanomolecules for Biomedical Uses. *J. Alloys Compd.* **2006**, *408−412*, 400–404.
40. Hua, H.; Feng, L.; Zhang, X.-p.; Zhang, L.-f.; Jin, J. Anti-Angiogenic Activity of Julibroside J8, a Natural Product Isolated from Albizia Julibrissin. *Phytomedicine* **2009**, *16*, 703–711.
41. Alley, M. C.; Hollingshead, M. G.; Pacula-Cox, C. M.; Waud, W. R.; Hartley, J. A.; Howard, P. W.; Gregson, S. J.; Thurston, D. E.; Sausville, E. A. SJG-136 (NSC 694501), A Novel Rationally Designed DNA Minor Groove Interstrand Cross-Linking Agent with Potent and Broad Spectrum Antitumor Activity: Part 2: Efficacy Evaluations. *Cancer Res.* **2004**, *64*, 6700–6706.